Available online at www.sciencedirect.com

ScienceDirect

Mendeleev Commun., 2020, **30**, 512–515

Mendeleev Communications

Formation of 2D calcium hydroxyapatite on stainless steel modified with a TiN sublayer

Vilma Jonauske,[a] Rimantas Ramanauskas,[b] Rasa Platakyte,[c] Gediminas Niaura,[b,c] Lina Mikoliunaite,[a,b] Kunio Ishikawa[d] and Aivaras Kareiva*[a]

[a] *Institute of Chemistry, Vilnius University, LT-03225 Vilnius, Lithuania. E-mail: aivaras.kareiva@chgf.vu.lt*
[b] *Center for Physical Sciences and Technology, LT-10257 Vilnius, Lithuania*
[c] *Institute of Chemical Physics, Vilnius University, LT-10257 Vilnius, Lithuania*
[d] *Department of Biomaterials, Faculty of Dental Science, Kyushu University, Maidashi, Higashi-Ku, Fukuoka 812-8582, Japan*

DOI: 10.1016/j.mencom.2020.07.037

The thin films of calcium hydroxyapatite were deposited on a stainless steel substrate modified with titanium nitride (TiN) using an aqueous sol–gel method and characterized by X-ray diffraction analysis. It was demonstrated for the first time that the formation of calcium hydroxyapatite during heat treatment inhibited the formation of Fe_2O_3 and promoted the formation of TiO_2 on the surface.

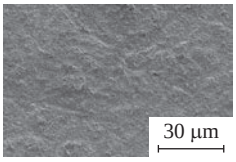

SEM micrograph of the sol–gel derived CHAp coatings on the 316L steel substrate with a TiN sublayer

Keywords: calcium hydroxyapatite, sol–gel synthesis, thin films, spin coating, TiN sublayer.

Due to the incidence of osteoarthritis and osteoporosis, the replacement of bones with implants is very common surgery.[1,2] Most of the implants (~80%) are made of metals due to their perfect mechanical properties, resistance to corrosion and acceptable biocompatibility; however, only a limited number of them are suitable for long-term applications.[3,4] Stainless steel, titanium, and cobalt–chromium and titanium alloys are most popular for implants.[5–7] In particular, 316L stainless steel is a preferred material for medical and dental applications.[8–11]

Because an implant is a foreign material for the human body, its surface properties have a huge impact on the behavior of bone cells that come into contact with implants.[12–14] The use of calcium hydroxyapatite [$Ca_{10}(PO_4)_6(OH)_2$, CHAp] supported on a metallic implant can reduce patient recovery times from 100 days with an uncoated implant to only 20 days with a CHAp-coated implant after implantation.[10] CHAp is suitable for bone substitution due to similar chemical composition and crystal structure.[15,16] However, the brittleness and poor mechanical properties of CHAp ceramics limit their application to the replacement of small non-load-bearing bone parts.[17] In order to overcome this disadvantage, CHAp is used as a thin coating on metallic implants.[18–20]

The surfaces of substrates should be modified to improve the properties of CHAp films, such as poor adhesion, high dissolution, and poor wear resistance, and to enhance the biocompatibility of metal implants.[21–26] The sol–gel preparation of thin films has the following advantages: simplicity, synthesis at low temperatures, effectiveness, suitability for complex-shaped implants, chemical homogeneity, fine grain structure of the end product and cost efficiency.[27–30] The aim of this study was to develop CHAp coatings on 316L stainless steel substrate modified with TiN sublayer using a sol–gel procedure.[†]

Figure 1[‡] shows the XRD patterns of CHAp films synthesized using spin-coating technique on the surface of 316L stainless steel modified with a TiN sublayer. According to the XRD data, iron was oxidized to a mixture of iron oxides with a dominating crystalline Fe_2O_3 phase upon heating the substrate at 850 °C in air.[31] Moreover, reflections due to TiN or oxidized TiO_2 phases could not be detected after a heat treatment of the substrate, probably, because of very intense reflections of iron oxides.[32] On the other hand, the TiO_2 formed could come off the surface upon the annealing of a 316L steel substrate modified with TiN. The XRD pattern of a CHAp sample obtained after one spinning procedure

[†] Calcium acetate monohydrate (99.9%) from Fluka, phosphoric acid (85.0%) from Reachem, 1,2-ethanediol (99.0%) from Alfa Aesar, ethylenediaminetetraacetic acid (EDTA) (99.0%) from Alfa Aesar, triethanolamine (TEA) (99.0%) from Merck, and poly(vinyl alcohol) (PVA) (99.5%) from Aldrich were used for the preparation of CHAp coatings on AISI 316L stainless steel rounds (10 × 0.5 mm) with TiN (2–3 μm) coating from Goodfellow. The TiN-modified substrates were washed with acetone in an ultrasonic cleaner for 15 min and then air dried before coating. Calcium acetate monohydrate and phosphoric acid were used for the synthesis of CHAp coatings. Calcium acetate monohydrate (5.2854 g, 0.03 mol) was dissolved in distilled water (40 ml), and 1,2-ethanediol (4 ml) was added. EDTA (9.6439 g, 0.033 mol) deprotonated with TEA (24 ml) was slowly added to this solution. After stirring for 10 h, phosphoric acid (1.23 ml) diluted with distilled water (20 ml) was added to the initial solution. After stirring for 24 h, the resulting gel (25 ml) was mixed with a 3% solution of PVA (15 ml). The mixture was stirred in a beaker covered with watch glass at room temperature and used for the synthesis of CHAp films on the TiN-modified stainless steel substrate using a spin-coating technique. For spin-coating, ~0.5 ml of a starting solution was applied to the stainless steel surface modified with a TiN sublayer using a syringe and then spin coated at 2000 rpm for 60 s in air. The substrates were repeatedly coated (1 to 10 times) according to the same procedure and each time annealed at 850 °C for 5 h in an oven.

[‡] X-ray diffraction (XRD) analysis was performed with a D8 Focus diffractometer (Bruker) with a LynxEye detector (Bruker) using CuKα radiation. The measurements were recorded at a step width of 0.02° and a speed of 1.5 deg min^{-1}.

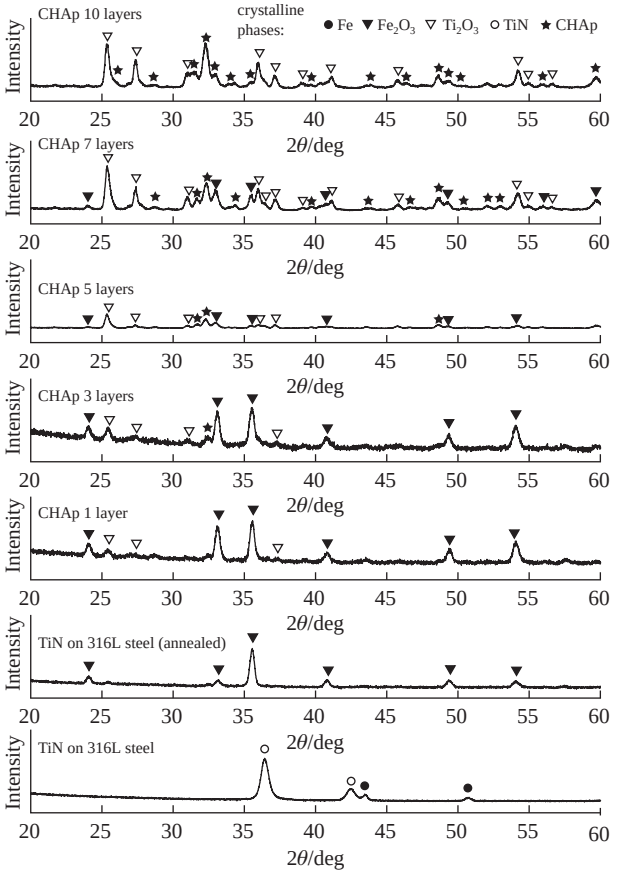

Figure 1 XRD patterns of CHAp films with various number of Ca–P–O gel layers synthesized on the 316L stainless steel surface modified with TiN.

already contained the reflections of iron and titanium oxides; thus, combustion in the course of sol–gel processing promoted the oxidation of TiN. Moreover, the sol–gel coating of CHAp also protected the mechanical integrity of formed TiO_2. The XRD pattern of a sample synthesized using three spinning and annealing steps exhibited a negligible reflection due to the CHAp phase. A further increase in the spinning and annealing times resulted in a monotonic increase in the intensities of reflections due to the crystalline phase of CHAp on the Fe/TiN substrate. In this case, the formation of CHAp presumably inhibited the formation of Fe_2O_3 and promoted the formation of TiO_2.

The SEM micrographs[§] of 316L steel substrates with TiN sublayers showed that the substrate surface before heat treatment was smooth, flat, and crack- and pore-free, but it was totally different after annealing the substrate at 850 °C. The surface during the heat-treatment was homogenously coated with differently shaped iron oxide microparticles with an average size of 1–2 μm. The porous microstructure of 316L steel substrates after the annealing was determined.[33] After the application of a first CHAp layer [Figure 2(*a*)], the microparticles of iron oxide were not merged anymore, and the less pronounced pores were filled with titania particles as expected (according to the XRD data). The situation slightly changed after the spinning of three CHAp layers [Figure 2(*b*)], and the surface microstructure significantly changed after repeating the synthesis of CHAp five times [Figure 2(*c*)] with the formation of a dense surface having small irregular pores (about 200 nm). Moreover, the surface was covered with plate-like crystallites about 1–2 μm in size. An even more compact coating was obtained after applying seven sol–gel layers [Figure 2(*d*)].

[§] The morphology of the samples was studied using a SU-70 scanning electron microscope (SEM) (Hitachi) and a BioScope Catalyst atomic force microscope (AFM) (Bruker).

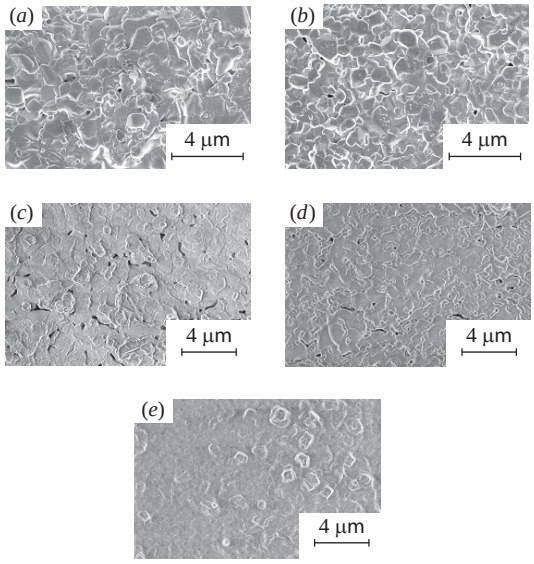

Figure 2 SEM micrographs of the sol–gel derived CHAp coatings on the 316L steel substrate with a TiN sublayer obtained after (*a*) 1, (*b*) 3, (*c*) 5, (*d*) 7 and (*e*) 10 spinning and annealing procedures.

The plate-like particles were transformed to spherical nanoparticles at this stage of sol–gel processing[34] due to the intense formation of a crystalline CHAp phase visible in the XRD patterns. The SEM image of a CHAp sample with 10 layers [Figure 2(*e*)] indicated the formation of a uniform surface with exposed irregular crystallites. Thus, with increasing the spinning and annealing times from seven to ten, the previously observed nanoparticles showed a tendency of growth to bigger derivatives.

Figure 3 and Table 1 summarize the AFM images and the results of AFM surface roughness measurements of the CHAp-coated samples. The roughness of the CHAp coatings decreased almost

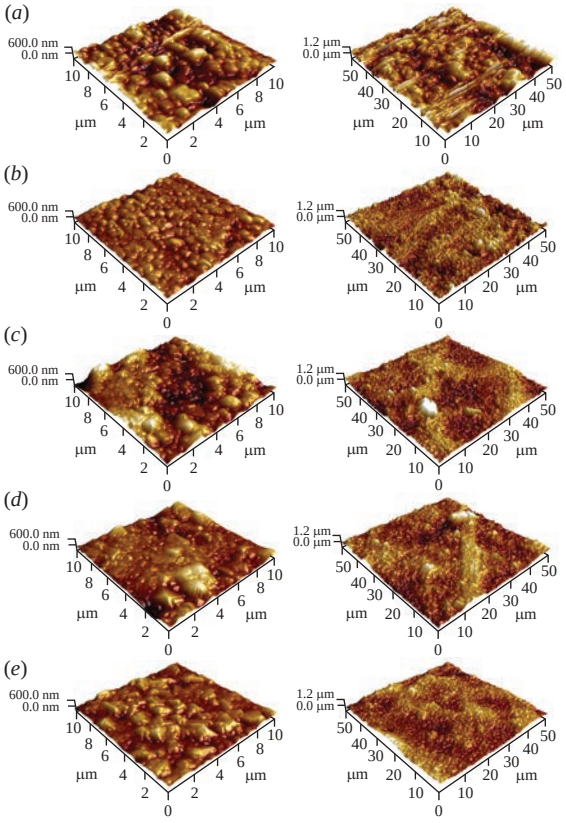

Figure 3 AFM images of different areas of CHAp samples obtained on the steel substrate with a TiN sublayer using (*a*) 1, (*b*) 3, (*c*) 5, (*d*) 7 and (*e*) 10 spinning and annealing procedures.

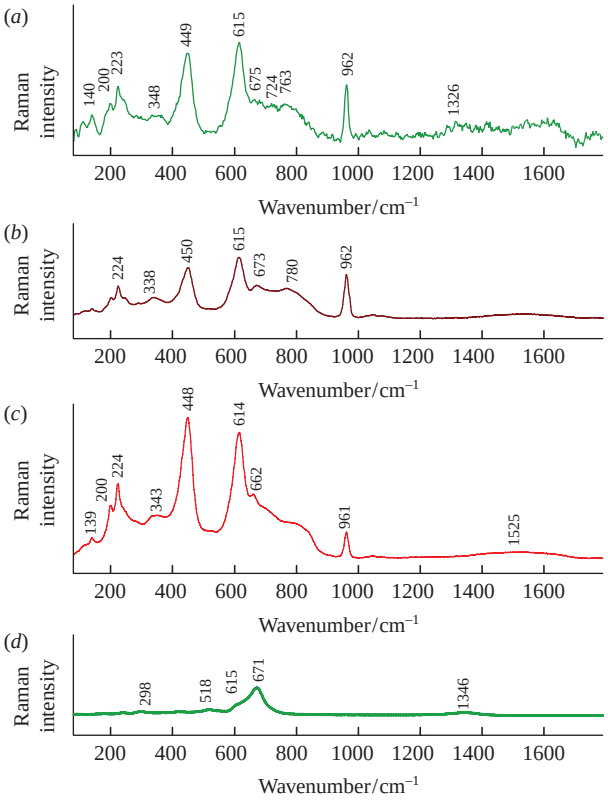

Figure 4 Raman spectra of samples containing (*a*) 10, (*b*) 7 and (*c*) 5 layers of a composition for the synthesis of CHAp deposited by spin coating and annealed at 850 °C and (*d*) the initial TiN/steel substrate before the deposition. Excitation wavelength: 532 nm (3 mW).

monotonically with the amount of CHAp layers. However, the CHAp coatings fabricated after three and five spinning and annealing times exhibited almost no changes in the roughness. This stage was the only one exception in the series of compounds. The AFM results are in a good correlation with those obtained by SEM measurements.

Figure 4 shows the Raman spectra[¶] of samples containing CHAp layers prepared by the spin-coating technique and subsequently annealed at 850 °C and a TiN/steel substrate before the formation of a hydroxyapatite coating. A dominant band at 671 cm^{-1} [Figure 4(*d*)] evidenced the presence of magnetite (Fe_3O_4) in the TiN/steel substrate.[35,36] A broad low-intensity band near 1346 cm^{-1} and a narrow low-intensity band at 298 cm^{-1} belonged to hematite (α-Fe_2O_3).[35,36] The formation of CHAp after the annealing of spin-coated precursors in the test samples [Figures 4(*a*)–(*c*)] is evident from a narrow and well-defined band at 961–962 cm^{-1}.[37] This band relates to the symmetric stretching vibrations ν_1 (A_1) of a tetrahedral phosphate group,[38] and it is characteristic of stoichiometric CHAp with a Ca/P molar ratio of 1.667.[37,38] Two intense bands at 614–615 and 448–450 cm^{-1} belong to TiO_2 rutile phase A_{1g} and E_g modes, respectively.[39,40] These bands indicated the conversion of a TiN layer into a TiO_2 rutile structure during the preparation of CHAp. Broad bands at 670–780 and 338–348 cm^{-1} can be related to maghemite (γ-Fe_2O_3).[35,36] Thus, the Raman-spectroscopic data fully supported the results obtained by XRD analysis. Interestingly, after ten coating procedures, the specific features attributable to the iron oxides are no longer visible in the XRD pattern and Raman spectrum are fully replaced by diffraction peaks and absorption bands of titanium oxide, respectively. Thus, the TiN sublayer acts as a buffer layer inhibiting the formation of iron oxides in the sol–gel synthesis of CHAp on the stainless steel surface and the formation of TiO_2/CHAp clusters.[41] Finally, the use of a stainless steel substrate modified with TiN for the preparation of CHAp coatings can improve the mechanical and anticorrosive properties and fretting resistance of the implants.[42]

In conclusion, an aqueous sol–gel method was applied to the synthesis of CHAp thin films on medical-grade stainless steel substrates with a TiN sublayer. Each layer in the preparation of CHAp multilayers was separately annealed at 850 °C in air. XRD analysis revealed that the CHAp phase is visible after five spin-coating and annealing procedures. With further increasing the number of spinning and annealing procedures, a monotonic increase of the intensities of reflections of the crystalline CHAp phase was observed in the XRD patterns of the films fabricated on a Fe/TiN substrate. It was demonstrated for the first time that the formation of CHAp inhibited the formation of Fe_2O_3 and promoted the formation of TiO_2 on the surface. The TiN sublayer acted as a buffer layer inhibiting the possible formation of iron oxides during the sol–gel synthesis. The AFM results for different areas showed that the roughness of the CHAp coatings on stainless steel with TiN sublayer substrates decreased almost monotonically with the amount of CHAp layers. These coatings of stoichiometric CHAp can be used to improve the integration of metallic implants in host bones.

A. K. acknowledges a fellowship administered by The Japan Society for the Promotion of Science (JSPS), Fellow's ID no. L12546. G. N. is grateful to the Center of Spectroscopic Characterization of Materials and Electronic/Molecular Processes (SPECTROVERSUM Infrastructure) for use of a Raman spectrometer.

References

1 R. J. Ferguson, A. J. Palmer, A. Taylor, M. L. Porter, H. Malchau and S. Glyn-Jones, *Lancet*, 2018, **392**, 1662.
2 C. Stewart, B. Akhavan, S. G. Wise and M. M. M. Bilek, *Prog. Mater. Sci.*, 2019, **106**, 100588.
3 M. Talha, Y. Ma, P. Kumar, Y. Lin and A. Singh, *Colloids Surf., B*, 2019, **176**, 494.
4 P. J. Andersen, in *Comprehensive Biomaterials II*, ed. P. Ducheyne, Elsevier, Oxford, 2017, pp. 1–18.
5 A. Balamurugan, S. Rajeswari, G. Balossier and A. H. S. Rebelo, *Mater. Corros.*, 2008, **59**, 855.
6 N. S. Manam, W. S. W. Harun, D. N. A. Shri, S. A. C. Ghani, T. Kurniawan, M. H. Ismail and M. H. I. Ibrahim, *J. Allois Compd.*, 2017, **701**, 698.
7 L. Yan, J. Yu, Y. Zhong, Y. Gu, Y. Ma, W. Li, J. Yan, Y. Ge, J. Yin, Y. Luo, A. Mirzasadeghi and Y. Yuan, *J. Nanosci. Nanotechnol.*, 2020, **20**, 1605.
8 I. Gurappa, *Surf. Coat. Technol.*, 2002, **161**, 70.
9 H. Khandelwal, G. Singh, K. Agrawal, S. Prakash and R. D. Agarwal, *Appl. Surf. Sci.*, 2013, **265**, 30.
10 D. T. M. Thanh, P. T. Nam, N. T. Phuong, L. X. Que, N. V. Anh, T. Hoang and T. D. Lam, *Mater. Sci. Eng., C*, 2013, **33**, 2037.
11 J. Zhao, Z. Zhai, D. Sun, C. Yang, X. Zhang, N. Huang, X. Jiang and K. Yang, *Mater. Sci. Eng., C*, 2019, **100**, 396.
12 F. A. Shah, P. Thomsen and A. Palmquist, *Acta Biomater.*, 2019, **84**, 1.
13 K. Sadtler, M. T. Wolf, S. Ganguly, C. A. Moad, L. Chung, S. Majumdar, F. Housseau, D. M. Pardoll and J. H. Elisseeff, *Biomater.*, 2019, **192**, 405.
14 H. Bretschneider, J. Mettelsiefen, C. Rentsch, M. Gelinsky, H. D. Link, K.-P. Günther, A. Lode and C. Hofbauer, *J. Biomed. Mater. Res., Part B*, 2019, **108**, 1117.
15 M. Vallet-Regi and J. M. Gonzalez-Calbet, *Prog. Solid State Chem.*, 2004, **32**, 1.
16 S. V. Dorozhkin, *Materials*, 2009, **2**, 1975.
17 H. Wang, Y. Li, Y. Zuo, J. Li, S. Ma and L. Cheng, *Biomaterials*, 2007, **28**, 3338.
18 V. Jonauske, A. Prichodko, R. Skaudzius and A. Kareiva, *Chemija*, 2016, **27**, 192.
19 G. Graziani, M. Boi and M. Bianchi, *Coatings*, 2018, **8**, 1.
20 P. Usinskas, Z. Stankeviciute, G. Niaura, J. Ceponkus and A. Kareiva, *Mater. Sci.-Medziagotyra*, 2019, **25**, 365.

[¶] The Raman spectra were recorded using an inVia Raman spectrometer (Renishaw) equipped with a thermoelectrically cooled (–70 °C) CCD camera and a microscope.

21 P. Usinskas, Z. Stankeviciute, A. Beganskiene and A. Kareiva, *Surf. Coat. Technol.*, 2016, **307**, 935.
22 P. Usinskas, Z. Stankeviciute, G. Niaura, J. Maminskas, G. Juodzbalys and A. Kareiva, *J. Sol-Gel Sci. Technol.*, 2017, **83**, 268.
23 A. I. Shaikhaliyev, A. A. Polisan, S. Y. Ivanov, Y. N. Parkhomenko, M. D. Malinkovich, K. N. Yarygin and L. D. Arazashvili, *J. Surf. Invest.: X-Ray, Synchrotron Neutron Tech.*, 2019, **13**, 644.
24 D. Sivaraj and K. Vijayalakshmi, *J. Anal. Appl. Pyrol.*, 2018, **134**, 176.
25 V. Jonauske, S. Stanionyte, S.-W. Chen, A. Zarkov, R. Juskenas, A. Selskis, T. Matijosius, T. C. K. Yang, K. Ishikawa, R. Ramanauskas and A. Kareiva, *Coatings*, 2019, **9**, 334.
26 C. J. Shuai, Y. L. Li, Y. W. Yang, S. P. Peng, W. J. Yang, F. W. Qi, S. X. Xiong, H. X. Liang and L. D. Shen, *Mater. Res. Express*, 2019, **6**, 115401.
27 S. V. Dorozhkin, *Acta Biomater.*, 2014, **10**, 2919.
28 G. J. Owens, R. K. Singh, F. Foroutan, M. Alqaysi, C.-M. Han, C. Mahapatra, H.-W. Kim and J. C. Knowles, *Prog. Mater. Sci.*, 2016, **77**, 1.
29 R. I. M. Asri, W. S. W. Harun, M. A. Hassan, S. A. C. Ghani and Z. Buyong, *J. Mech. Behav. Biomed. Mater.*, 2016, **57**, 95.
30 S. F. Robertson, A. Bandyopadhyay and S. Bose, *Surf. Coat. Technol.*, 2019, **372**, 140.
31 W. S. W. Harun, R. I. M. Asri, F. R. M. Romlay, S. Sharif, N. H. M. Jan and F. Tsumori, *J. Alloys Compd.*, 2018, **748**, 1044.
32 C.-C. Kuo, Y.-T. Lin, A. Chan and J.-T. Chang, *Coatings*, 2019, **9**, 555.
33 Z.-Q. Liu, J.-J. Han, Y. Su and Q.-L. An, *Proc. Inst. Mech. Eng., Part B*, 2018, **232**, 2488.
34 A. Ezerskyte-Miseviciene and A. Kareiva, *Mendeleev Commun.*, 2019, **29**, 273.
35 L. Bellot-Gurlet, D. Neff, S. Réguer, J. Monnier, M. Saheb and P. Dillmann, *J. Nano Res.*, 2009, **8**, 147.
36 P. Colomban, S. Cherifi and G. Despert, *J. Raman Spectrosc.*, 2008, **39**, 881.
37 M. Malakauskaite-Petruleviciene, Z. Stankeviciute, G. Niaura, A. Prichodko and A. Kareiva, *Ceram. Int.*, 2015, **41**, 7421.
38 G. Niaura, A. K. Gaigalas and V. L. Vilker, *J. Phys. Chem. B*, 1997, **101**, 9250.
39 L. Kernazhitsky, V. Shymanovska, T. Gavrilko, V. Naumov, L. Fedorenko, V. Kshnyakin and J. Baran, *Ukr. J. Phys.*, 2014, **59**, 246.
40 Y. Zhang, C. X. Harris, P. Wallenmeyer, J. Murowchick and X. Chen, *J. Phys. Chem. C*, 2013, **117**, 24015.
41 P. Allende, L. Barrientos, A. Orera, M. A. Laguna-Bercero, N. Salazar, M. L. Valenzuela and C. Diaz, *J. Cluster Sci.*, 2019, **30**, 1511.
42 A. Lanzutti, A. Raffaelli, M. Magnan, L. Fedrizzi, M. Regis and E. Marin, *Surf. Coat. Technol.*, 2019, **377**, 124895.

Received: 19th February 2020; Com. 20/6138